Energy Storage Materials 55 (2023) 587–596

Contents lists available at ScienceDirect

Energy Storage Materials

journal homepage: www.elsevier.com/locate/ensm

Tuning discharge voltage by Schottky electron barrier in P2-$Na_{2/3}Mg_{0.205}Ni_{0.1}Fe_{0.05}Mn_{0.645}O_2$

Yichao Wang [a], Zulipiya Shadike [b], William Fitzhugh [a], Fan Wu [a], Sang-Jun Lee [c], Jun-Sik Lee [c], Xi Chen [a], Yuanzheng Long [a], Enyuan Hu [d], Xin Li [a,*]

[a] John A. Paulson School of Engineering and Applied Sciences, Harvard University, Cambridge, MA 02138, USA
[b] Institute of Fuel Cells, School of Mechanical Engineering, Shanghai Jiao Tong University, Shanghai 200240, China
[c] Stanford Synchrotron Radiation Lightsource, SLAC National Accelerator Laboratory, Menlo Park, CA 94025, USA
[d] Chemistry Division, Brookhaven National Laboratory, Upton, NY 11973, USA

ARTICLE INFO

Keywords:
Na ion battery
Layered transition metal oxide
Phase evolution
Electronic structure
Schottky barrier

ABSTRACT

Recently, Mg doped Na metal oxide layered cathode compounds have attracted strong interest for Na-ion battery applications. Here a new type of asymmetric phase evolution between charge and discharge is found to show much-enhanced discharge voltage in P2-$Na_{2/3}Mg_{0.205}Ni_{0.1}Fe_{0.05}Mn_{0.645}O_2$ over the parent cathode compound. P2 solid solution is found to show an abnormal coexistence with O2-P2 two-phase reaction during discharge with simultaneous reduction of O, Ni, and Fe redoxes, distinct from the conventional P2-O2 two-phase reaction in the charge. Our analysis suggests that the P2 and O2 two-phase boundary forms a novel unidirectional Schottky barrier to impede electron and Na diffusions in discharge only, thus making the kinetically preferred P2 solid solution phase abnormally coexist with the two-phase region for high discharge voltage and low polarization. Our work demonstrates tuning dynamic evolution of electronic Schottky barrier as a new dimension for advanced kinetic design of high-performance battery cathode materials.

1. Introduction

Na ion battery (SIB) is a cost effective alternative to Li ion battery (LIB), especially for large scale energy storage that is sensitive to performance and cost ratios [1,2]. SIB's cathode has a broad choice of cheaper metal elements, including Na, Mg, Fe, Mn etc., which shows increasing advantage over LIB that faces the Co and Ni supply crisis [3–7].

Layered sodium transition metal (TM) oxide ($NaTMO_2$) is one of the most attractive families with abundant phases for many performance possibilities and for the opportunity to study novel phase evolutions [6–9]. From the perspective of charge-discharge structure evolution, $NaTMO_2$ can be divided into two main groups: P2-O2 and O3-P3, which follows Delmas et al.'s notation, where "P" or "O" indicates that Na ion resides in either prismatic or octahedral site of oxygen sublattice, and the following number 2 or 3 indicates that the hexagonal oxygen-ion layers follow AABB or ABCABC stacking [10].

Usually, common structural evolutions of $NaTMO_2$ between charge and discharge are either symmetric with reversible capacity or asymmetric with irreversible capacity. The former means $NaTMO_2$ goes through the same structure evolutions with symmetric electrochemical voltage curves between charge and discharge, and the latter usually suggests a destructive irreversible structure transformation when the cathode material is charged beyond a certain voltage, thus giving a very different discharge curve with significantly reduced capacity. However, we found that O3-$Na(Fe_xTM_y)O_2$ and O3-$NaMnO_2$ fall into a different category of the asymmetric structure evolution with a reversible capacity [6,7]. One critical factor that was found to give the asymmetry between charge and discharge in these materials is that the high-voltage phases show higher Na diffusivity than the phases at low voltage. The cathode materials once entered the phase of high ionic conductivity through battery charge thus want to stay longer in that phase during discharge due to the kinetic preference. It was found that these high-voltage phases are related to the advanced capacity, rate, or cyclability of the cathode materials.

We note that recent study of Mg-doped cathodes, P3-$Na_{2/3}Mg_{1/3}Mn_{2/3}O_2$, P2-$Na_{2/3}Mg_{0.28}Mn_{0.72}O_2$, and P2-$Na_{2/3}Ni_{1/3-x}Mg_xMn_{2/3}O_2$ ($x = 0.2$) also showed asymmetric charge-discharge curves and high

* Corresponding author at: 210 Pierce Hall, 29 Oxford St. Cambridge, MA 02138.
E-mail address: lixin@seas.harvard.edu (X. Li).

https://doi.org/10.1016/j.ensm.2022.12.027
Received 2 September 2022; Received in revised form 30 November 2022; Accepted 16 December 2022
Available online 17 December 2022

reversible capacity[11–15]. In P3-$Na_{2/3}Mg_{1/3}Mn_{2/3}O_2$ case, Song et al. used *ex situ* XRD refinement to characterize the phase evolution and found pure P3-O3 two phase reaction at the charge plateau, but in discharge the O3-P3 two-phase reaction happened together with an O3 solid solution at the initial stage, where Mg reversible migration was first speculated [14]. Later, P2-$Na_{2/3}Mg_{0.28}Mn_{0.72}O_2$ was found to show out-of-plane Mg migration in charge, followed by in-plane Mn reordering and molecular oxygen pairing. The in situ X-ray diffraction shows that O2 structure forms by P2-O2 two phase reaction during charge, while during discharge, the O2 phase undergoes solid solution reaction to transform back to P2 with an unusual partial recovery of the original Mg and Mn honeycomb ordering [15].

In this work, P2-$Na_{2/3}Mg_{0.28}Mn_{0.72}O_2$ (MgMn) and P2-$Na_{2/3}Mg_{0.205}Ni_{0.1}Fe_{0.05}Mn_{0.645}O_2$ (MgNiFeMn) were synthesized by conventional solid-state reactions. *Ex situ* X-ray diffraction (XRD) was used to examine the crystal phase evolutions of both materials and high-resolution transmission electron microscopy (HRTEM) imaging was performed to characterize high voltage phase of MgNiFeMn. *Ex situ* X-ray absorption spectroscopy (XAS) was conducted on both TM and O elements of MgNiFeMn to characterize the redox evolution. Together with *ab initio* simulations, we unveil the distinct origins of the asymmetries for both cases. In MgMn, a simpler scenario of reversible Mg migration, without Mn reordering or O molecular pairing, was found by our density functional theory (DFT) simulations, which well explains the asymmetric phase evolution and the partial recovery of the Mg/Mn honeycomb ordering. More interestingly, an abnormal P2 solid solution reaction was found to happen simultaneously with P2-O2 two-phase reaction in the discharge of MgNiFeMn, giving unusual asymmetry between charge and discharge and an obvious enhancement of discharge voltage and reduction of polarization over the parent compound of MgMn. A unidirectional electron Schottky barrier between semiconductive P2 phase and metallic O2 one is found to impede electron and thus Na diffusions in discharge only. The barrier causes the kinetically sluggish two-phase boundary evolution and gives a kinetic preference for the P2 solid solution phase to coexist. A general electrochemistry model is then proposed to quantitatively describe the competition between kinetics and thermodynamics for the asymmetric phase evolution in MgNiFeMn, paving the way for tuning the dynamic evolution of such a barrier by novel electronic and kinetic structure design, which can lead to enhanced discharge voltage and reduced polarization for high-performance sodium ion battery applications.

2. Results

Fig. 1a shows the powder XRD patterns of the as-synthesized MgMn and MgNiFeMn, which share hexagonal $P6_3/mmc$ space group. The XRD superstructure (1/3 1/3 0) peak corresponds to the AA stacking of TM honeycomb superstructure [11,16], which means it repeats itself every layer. MgNiFeMn shows smaller (1/3 1/3 0) peak than MgMn possibly due to the weaker degree of the honeycomb ordering. The small peaks in the 2-theta range of 25 to 30° for MgMn are also from TM honeycomb superstructure that has been well identified previously. In addition, our DFT simulations show that the AA stacking is 7 meV/TMO_2 and 4 meV/TMO_2 lower in energy than the AB stacking for MgNiFeMn and MgMn, respectively.

Fig. 1b shows the electrochemical charge-discharge curves of MgMn and MgNiFeMn in the voltage range of 1.5 V to 4.4 V at 0.1C. During charge, they both show slope region followed by a high voltage plateau, but both plateaus disappeared during discharge, giving asymmetries between charge and discharge. In addition, the discharge voltage is obviously much higher in MgNiFeMn than MgMn. Fig. S1a shows the cycling performance of the two materials with MgNiFeMn showing a superior cycling than MgMn. As shown in Figs. S1b,c, in the following cycles, the high voltage plateau becomes much shorter for MgMn in charge due to the increase of Mg/Mn reordering[15], while there is only a gradual change of slope for MgNiFeMn, which could be partially caused by the gradual increase of irreversible stacking faults[11].

First, to better compare with MgNiFeMn later and understand their difference in asymmetric charge-discharge curves, ex situ XRD was conducted to characterize the crystal phase evolution of MgMn. Figs. 2a and 2b show the first cycle crystal phase evolution of MgMn. During charge, in the slope region from open circuit voltage (OCV) up to 4.2 V, only relative shift of P2 002 peak is observed, suggesting a solid solution phase. In the plateau region from 4.2 V to 4.4 V, P2 002 peak stops shifting and a second peak at 18° corresponding to O2 002 reflection appears as indicated by the yellow dash line in Fig. 2b, suggesting P2-O2 two-phase reaction [11]. However, during discharge, the O2 002 peak shift is observed from XRD within 70 mAh/g discharge capacity as indicated by the blue dash line, suggesting solid solution reaction in the newly formed O2 phase in discharge. When it is further discharged to 2.2 V of the same Na composition as the pristine state, the O2 002 peak disappears and the pure P2 phase is regained. The ex situ XRD analysis here thus confirms the asymmetric crystal phase evolution for MgMn with reversible capacity, as summarized in Fig. 2a. O2 is formed through P2-O2 two-phase reaction during charge, but rather than disappearing symmetrically through O2-P2 two-phase reaction in discharge, the O2

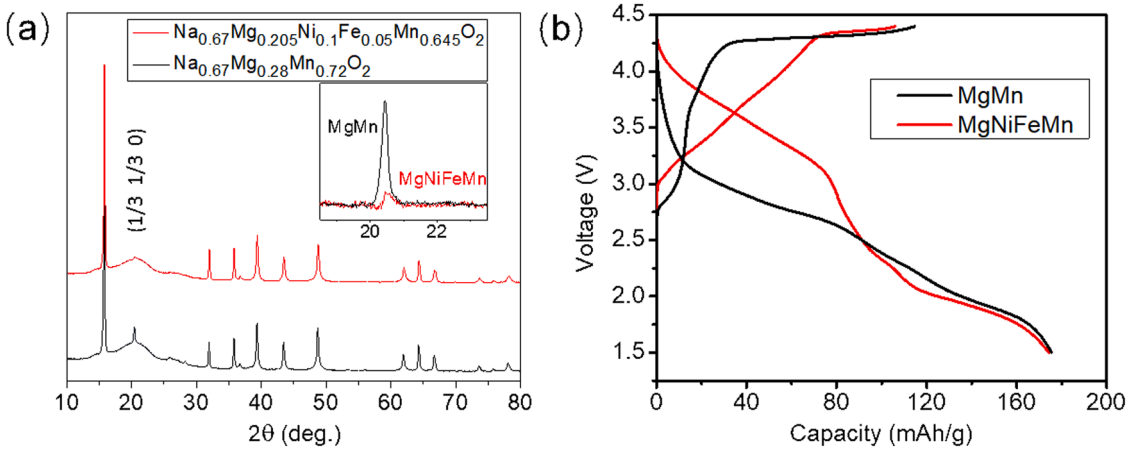

Fig. 1. Structure and voltage profile comparison between MgMn and MgNiFeMn. (a) X-ray diffraction patterns comparison for P2 phase of $Na_{2/3}Mg_{0.28}Mn_{0.72}O_2$ (MgMn) and $Na_{2/3}Mg_{0.205}Ni_{0.1}Fe_{0.05}Mn_{0.645}O_2$ (MgNiFeMn). The peak labelled by (1/3 1/3 0) represents the Mg(Ni)/Mn TM ordering related superstructure peaks. The inset zooms in the region after background subtraction. **(b)** Comparison of voltage curves between MgMn and MgNiFeMn in the voltage range of 1.5–4.4 V at 0.1C.

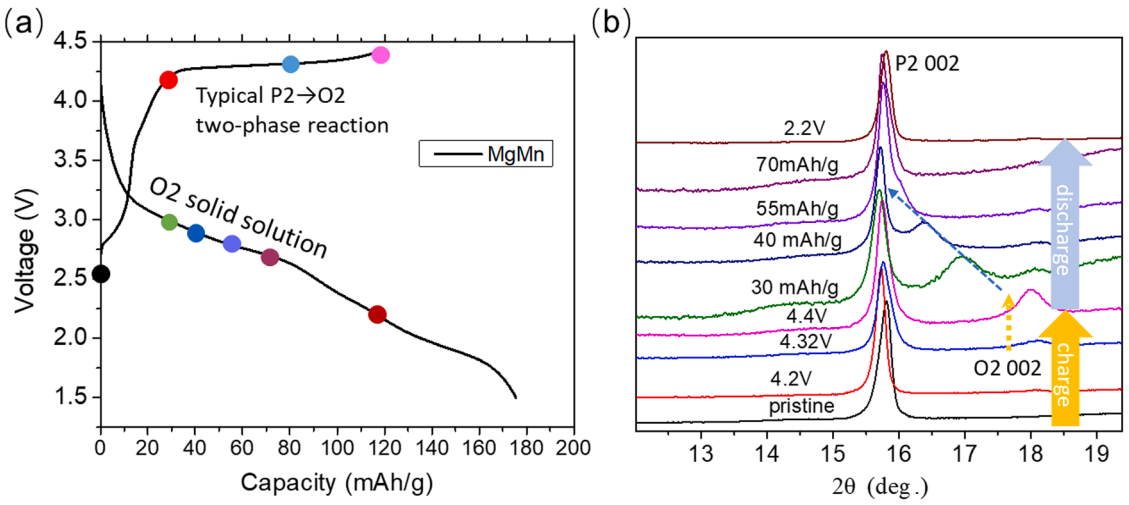

Fig. 2. First cycle crystal phase evolution of MgMn. (a) Charge-discharge curve with colored dots indicating the states of charge at which the ex situ XRD patterns were collected; **(b)** XRD patterns labeled with the same color in 2(a) and with the states of charge in volt or mAh/g, with 2θ ranging from 12° to 19.5°, including 002 reflections for P2 and O2. The yellow and blue dash lines represent the 2θ shift of the O2 002 reflection.

phase first deintercalates Na ions through solid solution and then transforms abruptly back to P2 beyond a certain Na composition, giving the asymmetry to the charge evolution.

To further understand the mechanism of the asymmetric crystal phase evolution, a series of DFT relaxations were designed for various MgMn structures. In Fig. 3a, we created a O2 structure with Na composition of 1/9 and *c* value of 9.84 Å calculated from the 18° O2 002 peak. After DFT relaxation, Mg ions automatically migrate to tetrahedral sites in Na layers. We further created two O2 structures without and with Mg migration, respectively, as shown in the left panels of Figs. 3b and 3c.

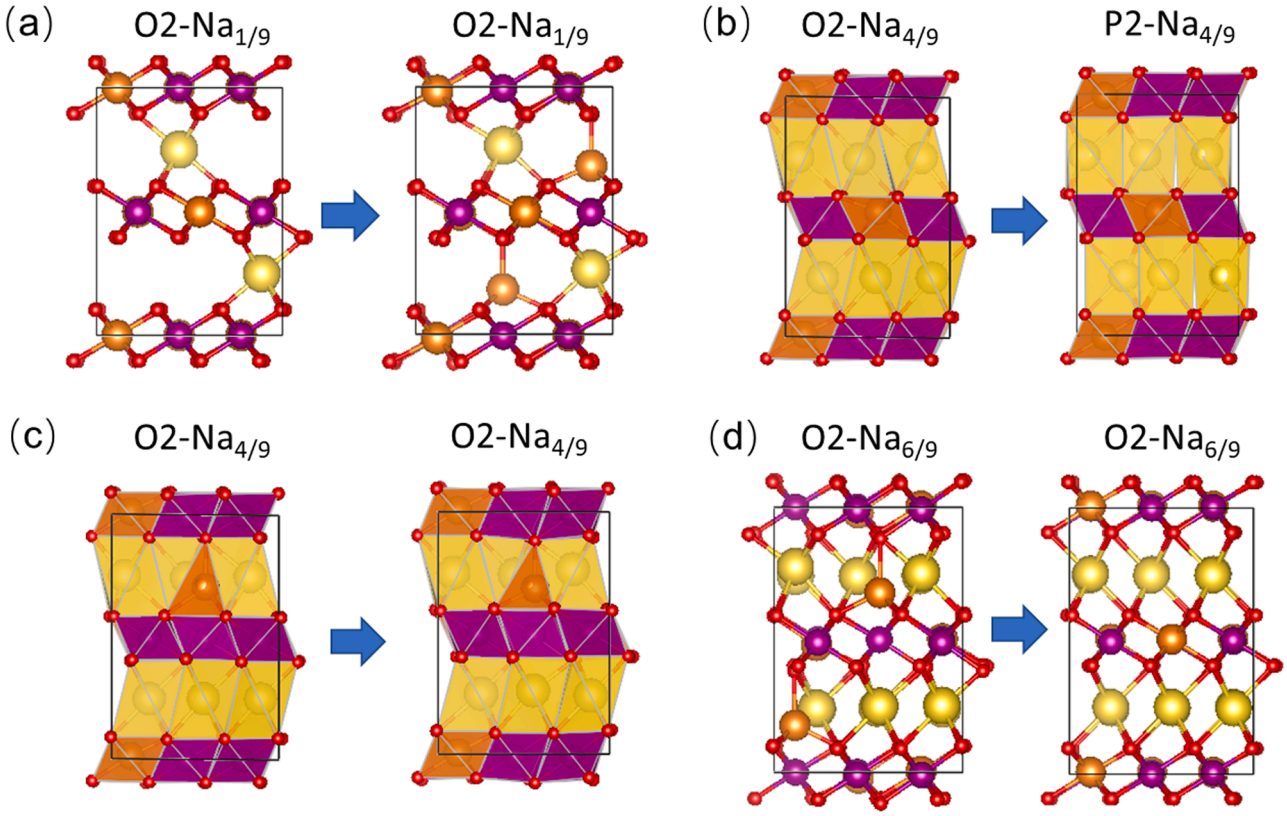

Fig. 3. Mg migration related DFT simulations in MgMn. The manually created crystal structures are on the left side of each panel, which transforms along the blue arrow by DFT full relaxation to the ones on the right. **(a)** In the starting O2 structure, Na composition is 1/9 and lattice parameter c is set to 9.84 Å. After relaxation, Mg ion migrates from TM layer to the neighboring Na layer when the face sharing octahedral site on the other neighboring Na layer is occupied by a Na ion; **(b)** In the starting O2 structure, Na composition is 4/9 and Mg ions stay in TM layers. After relaxation, O2 automatically transforms to P2; **(c)** The starting O2 structure is the same as in 3(b) except that each Na layer is with one migrated Mg ion in the tetrahedral site. Note that the migrated Mg in the bottom Na layer is visually blocked by Na ions. After relaxation, Mg ions stay in tetrahedral sites and the O2 structure is maintained; **(d)** In the starting O2 structure, each layer has a migrated Mg ion, and the Na composition is 2/3. After relaxation, Mg ions migrate back to the TM layer.

The Na compositions are chosen to be 4/9 as the O2-P2 two-phase reaction usually happens higher than the Na composition of 1/3 in MgMn [17]. After relaxation, the O2 structure without Mg migration converts to P2 automatically (Fig. 3b), but the structure with Mg migration is not relaxed to P2 structure and the O2 stacking is maintained (Fig. 3c). When the Na composition is increased to 2/3 in the structure of our DFT simulation, as shown in Fig. 3d, we find that the migrated Mg is automatically relaxed back to the TM layer.

From our XRD and DFT results, the asymmetric phase evolution of MgMn cathode between charge and discharge is related to the reversible Mg migration in the O2 phase. The migration is formed in the O2-P2 two phase region in charge, which stabilizes the O2 stacking in discharge for a solid solution phase and thus avoids the O2-P2 two-phase reaction. Toward the end of discharge, when sufficient Mg ions are pushed back to the TM layer by high enough Na composition, the impedance for O2 transforming back to P2 is thus lifted and the system goes back to a pure P2 phase abruptly. Note that this simpler mechanism of Mg reversible migration here is truly reversible and does not involve Mn reordering. Thus, it can better recover the original honeycomb ordering between Mn and Mg in discharge, as found in experiment previously. The gradual loss of such a honeycomb ordering upon cycling, however, could be caused by the growth of phase regions with additional mechanisms of less reversible Mg migration, such as the one accompanied with Mn reordering and O—O pairing [15].

Now we focus on understanding the structure evolution underlying the charge-discharge curves of MgNiFeMn. We first conducted ex situ XRD during charge. The slope region from OCV to 4.3 V corresponds to a normal solid solution phase of P2 as shown in Fig. S2, while we are more interested in the property of the voltage plateau above 4.3 V. Fig. 4a shows the voltage states at which XRD patterns were measured on the plateau and Fig. 4b shows the corresponding 002 peaks. At 4.3 V, the XRD pattern confirms that it is P2 structure (Fig. S2, Fig 4b). As the charge further proceeds into the plateau region, the 002 peak becomes right skewed (Fig. 4b). Rietveld two-phase refinement was used to refine

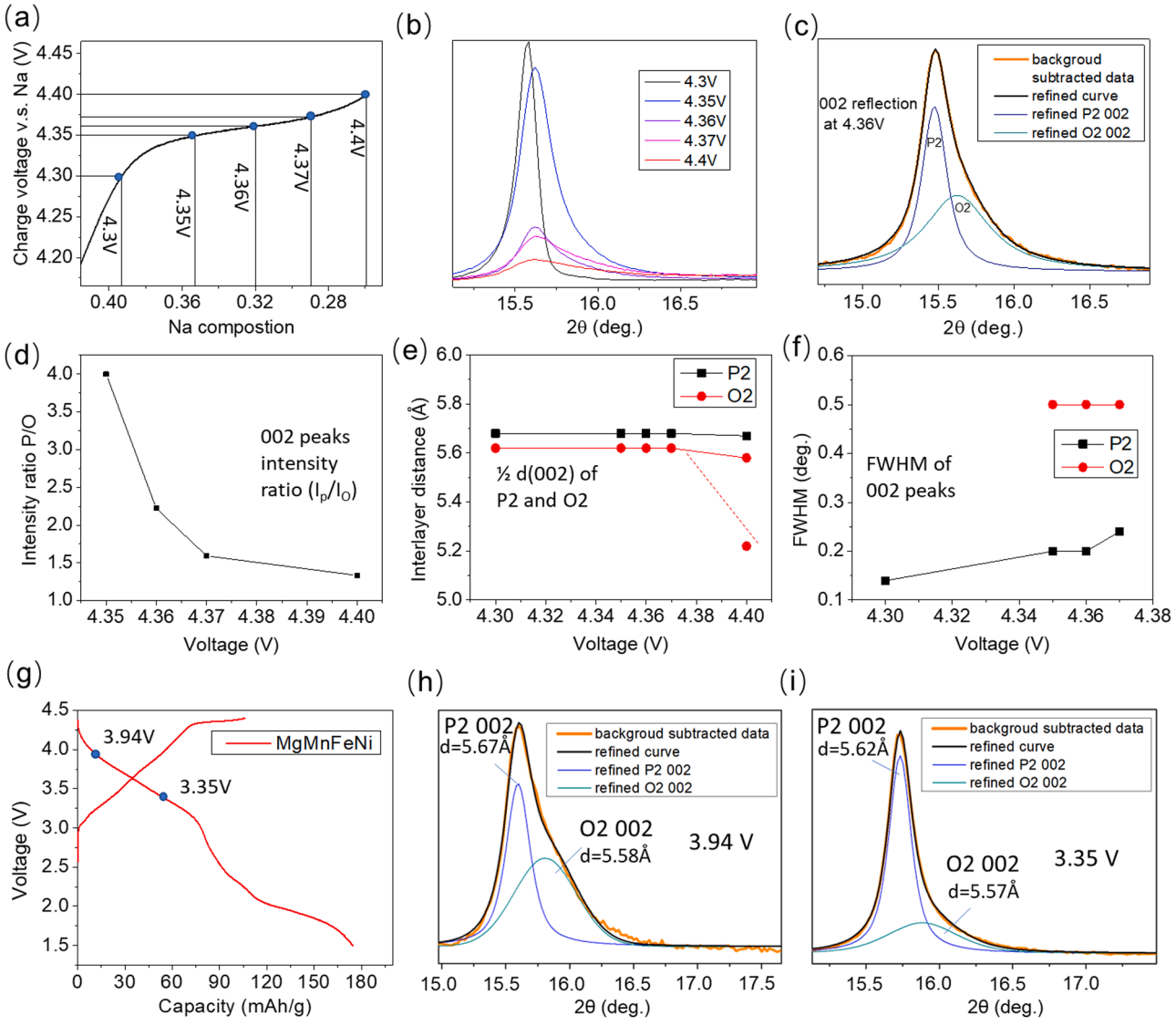

Fig. 4. Crystal structure evolution of MgNiFeMn during high voltage plateau and discharge voltage slope characterized by ex situ XRD and refinement. (a) Charge curve above 4.2 V with the blue dots indicating the five charged states where the XRD patterns were collected; **(b)** the 002 reflections of the five charged states at the voltage plateau > 4.2 V, where the 002 peak intensity is reduced with charging; **(c)** two-phase refinement illustrated using the 4.36 V XRD pattern with P2 and O2 phases. The orange, black, blue, and green lines are the background subtracted data, refined curve, refined P2, and refined O2 phases, respectively; **(d)** The intensity ratio of the 002 peaks between P2 and O2 phases versus charge states; **(e)** interlayer distance evolution of P2 and O2 phases; **(f)** Full width at half maximum (FWHM) evolution of 002 peaks of P2 and O2; **(g)** Charge-discharge curves with dots indicating the states of charge where the XRD patterns were collected; **(h, i)** XRD patterns of 002 reflections at 3.94 V and 3.35 V, respectively, together with the two-phase refinement with P2 and O2 phases.

the full pattern from 10 to 80° into P2 and O2 phases. Fig. 4c shows an example of the refinement at 4.36 V, where the refined Gaussian type of 002 peaks from P2 and O2 in superposition agrees well with experiment. Fig. 4d shows a decreasing trend of the refined intensity ratio between P2 and O2 002 reflections, suggesting that the charge process consumes P2 and grows O2 phases. Fig. 4e shows the mostly unchanged layer distance on the plateau except for the end of charge at 4.4 V, indicating unchanged Na composition in each phase for a typical two-phase reaction. The XRD pattern of the 4.4 V state is shown in Figure S2, where the abrupt change of O2 interlayer distance at 4.4 V is probably due to certain amount of O2 solid solution. Fig. 4f shows the FWHM evolution of 002 reflections on the plateau, where the P2 002 keeps broadening and O2 002 does not change, indicating that the size of each P2 region is decreasing but that of O2 region does not change. This suggests that for a given particle the P2 region is consumed by the simultaneous emergence of multiple similar O2 regions. Fig. 4d-f suggest that the plateau region in battery charge is mainly a typical two-phase reaction between P2 and O2 phases.

Figs. 4g-i show the structure evolution during discharge of MgNiFeMn. Fig. 4g shows the voltage position where XRD patterns were measured. Figs. 4h and 4i show the corresponding 002 reflections together with the two-phase XRD refinement from the full two-theta range of 10 to 80°. At the beginning of discharge at 3.94 V the reflection is mainly contributed by two 002 peaks of P2 and O2 phases, with interlayer distance of 5.67 Å and 5.58 Å, respectively (Fig. 4h). When being further discharged to 3.35 V, the right skew of 002 peak is less obvious but still exists (Fig. 4i), suggesting that the O2 phase has largely been transformed back to P2 phase through a two-phase reaction, but the reaction has not been finished yet. Surprisingly, the refinement also shows that the interlayer distance of P2 is 5.62 Å at 3.35 V in discharge, which is lower than that of both 3.94 V at the beginning of discharge and 3.7 V state during charge as shown in Fig. S2, suggesting an increase of the Na composition in the P2 phase in discharge. Using the relationship between capacity, voltage, and interlayer distance found in charge in the P2 solid solution phase (Fig. S2), it can be estimated that more than 12% of Na vacancy in P2 becomes occupied in the discharge from 4.4 V to 3.35 V through an abnormal solid solution reaction, because it happens in parallel with the O2-P2 two-phase reaction (Fig. 4g-i).

To further understand atomic details of the P2-O2 two-phase region, we used HRTEM to directly imaging the MgNiFeMn sample along *b* direction charged at 4.4 V as shown in Fig. 5a. Fig. 5b further labeled different colors for different phases and phase boundaries, where blue dots follow the P2 TM stacking with TM largely repeats itself every layer along *c* direction, and orange dots follow the O2 TM stacking with the neighboring TM layers apparently gliding in a-b plane relatively and repeating itself only every other layer along *c* direction. We find that P2 and O2 regions can share one TM layer and form a two-phase boundary region that gradually transits between the two phases using several transition metal atomic columns (green regions in Fig. 5b). The fact that such a P2-O2 phase boundary can exist is probably due to very close interlayer distances between the two phases, so that the mismatch strain is small.

The XRD and HRTEM in Figs. 4 and 5 together confirm that during charge of MgNiFeMn the P2 solid solution (slope region below 4.3 V) and P2-O2 two-phase reaction (plateau region from 4.3 V to 4.4 V) occur separately. The high voltage plateau mainly corresponds to a typical two-phase reaction between P2 and O2, where they coexist in one TM layer with the phase boundary region of less than 10 TM atomic columns to make the gradual transition between the two phases. However, once such a seemingly normal two-phase structure is formed in charge, abnormal asymmetry in discharge is observed, where O2-P2 two-phase and P2 solid solution reactions occur simultaneously in a voltage slope region without any obvious voltage plateau.

We further investigate whether the redox evolution is also asymmetric between charge and discharge. Fig. 6 shows the result of ex situ X-ray absorption near edge structure (XANES) spectra of Ni K-edge and Fe K-edge. Mn K-edge spectra are also measured as shown in Fig. S3, which does not shift much at a voltage range higher than 2.23 V. Fig. 6a shows the voltage states where XAS are measured. Fig. 6b summarizes the shift of XAS at half edge jump obtained from the XAS of Ni and Fe during charge and discharge shown in Fig. 6c-f. The asymmetric redox evolution of both Ni and Fe are obvious in Fig. 6b. During charge, their K-edges make continuous fast shift towards higher energy below 4 V but barely shift above 4.3 V, indicating that Ni and Fe are only oxidized below 4.3 V in the P2 solid solution phase, while they are barely oxidized during the charge plateau above 4.3 V for the two-phase reaction discussed in Fig. 4. However, during discharge, they immediately shift towards lower energy, suggesting that they are reduced throughout the whole discharge process to 2.23 V, consistent with the slope discharge voltage profile analyzed in Fig. 4g-i. The shape change of Fe edge can arise from structure change, oxidation of the hybridized FeO_6 octahedra, and/or $Fe^{3+/4+}$ redox. The $Fe^{3+/4+}$ redox in Na cathode materials was characterized by XAS together with Mössbauer spectroscopy in P2-$Na_xFe_{0.5}Mn_{0.5}O_2$[3], $NaFe_{0.3}Ni_{0.7}O_2$[18], and $Na_{0.61}[Mn_{0.27}Fe_{0.34}Ti_{0.39}]O_2$[19]. Specifically, in $Na_{0.61}[Mn_{0.27}Fe_{0.34}Ti_{0.39}]O_2$, an ~1 eV half edge jump shift of XAS for $Fe^{3+/4+}$ redox was simultaneously confirmed by Mössbauer spectroscopy, which is consistent with the amount of shift observed in our MgNiFeMn (Fig. 6b and insets in Fig. 6e and f). Moreover, the shortening of Fe-O bond as shown in the extended X-ray absorption fine structure analysis (added Fig. S4) further suggests the oxidation of Fe^{3+} during charge, and vice versa for that during discharge. However, due to the hybridization of Fe3d with O2p orbitals, the partial contribution from oxygen redox, as we will show in Fig. 7, cannot be excluded.

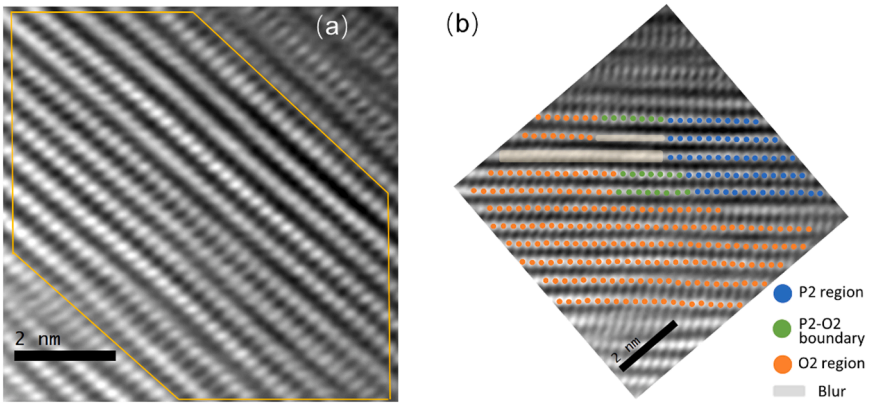

Fig. 5. HRTEM in *b* direction of a cathode particle charged to 4.4 V. (a) HRTEM with FFT filter; **(b)** HRTEM labeled with blue dots for P2 region, orange dots for O2 region, green dots for P2-O2 boundary region, and gray rectangle for blurry region.

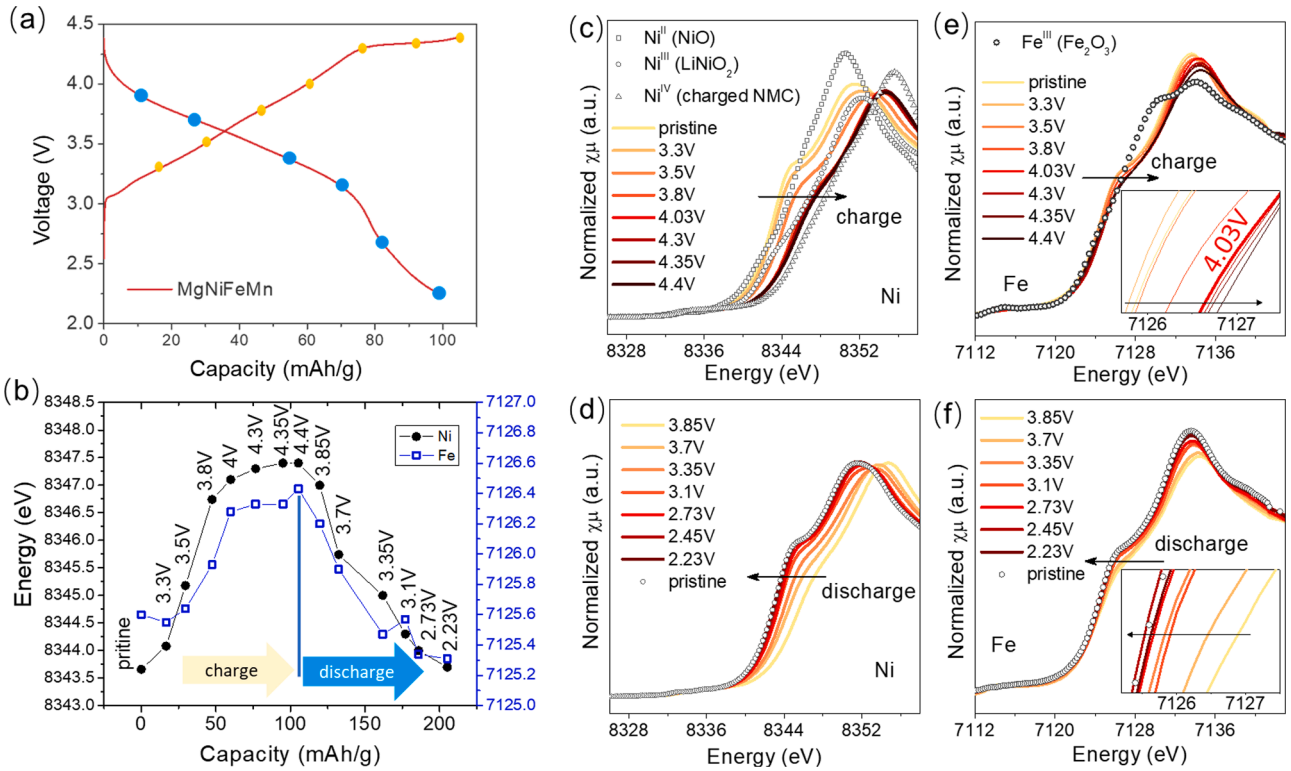

Fig. 6. Ex situ XANES measurement of Ni and Fe in MgNiFeMn. (a) Charge-discharge curve with dots indicating the states at which the XAS patterns were collected; **(b)** Summary of peak energy evolution of the XANES of Ni and Fe during charge-discharge; **(c, d)** XANES evolution of Ni during charge and discharge; **(e, f)** XANES evolution of Fe during charge and discharge. The insets enlarge the half edge jump region labeled by the arrow.

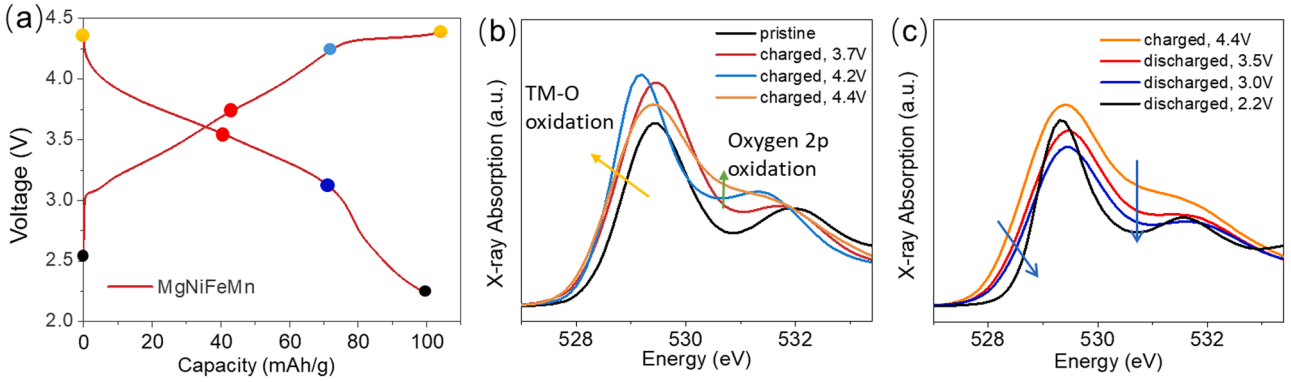

Fig. 7. Ex situ soft-XAS of oxygen K-edge during charge and discharge of MgNiFeMn. (a) Charge-discharge curves with colored dots indicating the charge states at which the XAS were measured; **(b)** Oxygen K-edge evolution during charge. The left shift of the rising edge labeled by the yellow arrow indicates TM-O oxidation mainly from pristine OCV to 3.7 V and the absorption increase at around 530.6 eV labeled by the green arrow indicates pure oxygen 2p hole oxidation mainly above 3.7 V; **(c)** Oxygen K-edge evolution during discharge. The right shift of the rising edge and decrease of the energy at about 530.6 eV labeled by two blue arrows happen simultaneously throughout discharge.

We also used soft-XAS of oxygen K-edge to characterize the oxygen redox evolution. Fig. 7 shows the ex situ XAS of oxygen K-edge during charge and discharge. Fig. 7a shows the voltage states where the XAS were measured, and Figs. 7b and 7c show the corresponding XAS during charge and discharge, respectively. In Fig. 7b, the rising edge of the pre-edge in charge shifts to lower energy between pristine state and 3.7 V state, as labeled by the yellow arrow, which is a common trend when TM-O hybridized states are oxidized and Fermi level is lowered, causing a lower energy that is needed to excite 1 s core electron of oxygen. This is consistent with the right shift of Ni and Fe K-edge XANES during slope region of charge. In Fig. 7b from 4.2 V to 4.4 V, the pre-edge is broadened and the intensity at around 530.6 eV increases, corresponding to oxidation of non-bonding oxygen 2p states [20]. During discharge, the first XAS is measured at 3.5 V, where the Na composition is actually between the two states represented by red and blue dots around 3.7 V during charge. We notice that although the rising edges do not have obvious shift during charge beyond 3.7 V, it has already been shifted to higher energy in discharge from 4.4 V to 3.5 V, which is consistent with the participation of Fe and Ni redox during initial discharge observed in XANES measurement. The intensity at 530.6 eV continuously decreases, and at 2.23 V the XAS of oxygen K-edge is largely recovered to the pristine state, as shown in Fig. S5, indicating good reversibility of the oxygen redox.

Figs. 6 and 7 together illustrate that, during charge the TM (Fe and Ni) redoxes and oxygen redox contribute to the capacity of the slope P2 solid solution region below 4.3 V and the plateau two-phase region

above 4.3 V, separately, while throughout discharge, TM redoxes are active all the time, along with reversible oxygen redox. Therefore, the redox evolution of MgNiFeMn is also asymmetric between charge and discharge, which is different from MgMn that shows symmetric redox sequence as previously reported[12,15]. Furthermore, our tested battery capacity of 106 mAh/g at 2.23 V discharge cutoff shows that the extra capacity of 39 mAh/g over the theoretical capacity of 67 mAh/g calculated based on the TM redox is almost exactly the capacity of the high voltage plateau above 4.3 V in charge (35 mAh/g), consistent with the reversible oxygen redox unveiled by XAS measurement.

3. Discussion

1. The asymmetric structure and redox evolutions of MgNiFeMn

The ex situ XRD and XAS results suggest that both crystal structure and redox sequence evolutions are asymmetric between charge and discharge for MgNiFeMn, as summarized in Fig. 8. During charge, the slope region corresponds to P2 solid solution with Fe and Ni redoxes, and the plateau region above 4.3 V corresponds to P2-O2 two-phase region with oxygen redox. Note that the capacity that has been charged from OCV to the beginning of the plateau at 4.3 V corresponds to about 27% Na extraction, which almost matches the theoretical capacity calculated based on $Ni^{2+/3+/4+}$ and $Fe^{3+/4+}$ redoxes (26%). This means that in principle no more TM redox will provide electrons during charge beyond this point, and oxygen redox has to be activated beyond 4.3 V in charge to provide electrons, all consistent with our XAS analysis. This is like some LIB Li-excess cathodes and SIB cathodes [12,20,21]. However, the abnormal phenomenon here is that the discharge shows a simultaneous mixture of P2 solid solution and O2-P2 two-phase reactions.

2. The electron Schottky barrier as origin of the asymmetry

There are several possible candidate mechanisms for the asymmetric behavior in MgNiFeMn. For example, TM migration in the O2 phase can modify the oxygen redox voltage, leading to such asymmetry [20]. But 5.6 Å interlayer distance here should be large enough to limit the TM migration. We relaxed two structures in DFT simulations with and without Mg migration with fixed lattice parameter and *c* being 11.2 Å. The Mg-migrated structure has 0.4 eV higher energy than the structure without Mg migration, suggesting an even higher Mg migration barrier around 0.6 to 0.8 eV. This is different from the Mg migration in other high voltage phases with much lower interlayer distance and hence lower Mg migration barrier[22]. Thus, although Mg migration happened spontaneously in MgMn in our DFT simulation, it does not prefer to happen in MgNiFeMn. The structure change of oxygen sublattice could be another possibility, such as O—O pairing [23]. However, O—O pairing will rely on Mg migration and Mn reordering in MgMn [15]. Since it's unlikely to have Mg migration in MgNiFeMn due to the high interlayer distances in both O2 and P2 phases, we do not consider O—O pairing as a possibility here. Inspired by the general idea of competition between kinetics and thermodynamics induced by ionic diffusivity related kinetics found in the Fe-rippling case[6] and the O3-$NaMnO_2$ case[7] mentioned in the introduction, here we propose a new model originated from Schottky-like electronic barrier to explain the asymmetric evolution found in MgNiFeMn, which is well distinguished from previous models related to ionic barriers only.

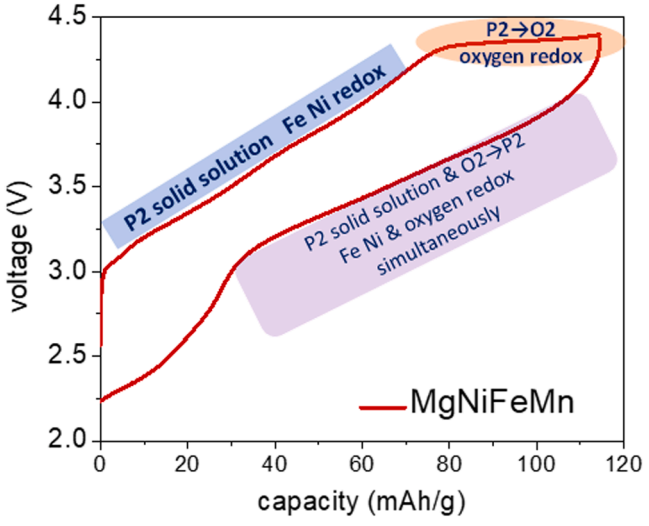

Fig. 8. Summary of asymmetric structure and redox evolutions during charge and discharge for MgNiFeMn.

From HRTEM, we've observed a P2-O2 boundary region between the two phases with similar interlayer distance. The phase transformation from P2 to O2 or from O2 back to P2 in the two-phase reaction should proceed through the movement of such boundaries [9]. During charge, the voltage plateau region above 4.3 V corresponds to a typical P2-O2 two phase reaction, suggesting a smooth phase boundary movement. However, during discharge, two-phase reaction occurs together with P2 solid solution, which should result from slow two-phase reaction impeded by sluggish phase boundary movement.

Since the redox sequence is found by us to be asymmetric in MgNiFeMn between charge and discharge, we now discuss a scenario about how the asymmetry in electronic structures could lead to an asymmetry in the phase boundary movement. Figs. 9a and 9b show the DFT calculated density of states (DOS) of O2 and P2 phases with Na composition of 2/9 and 4/9, respectively. Na composition of 2/9 is suitably chosen because it is just slightly below the Na composition at the end of the voltage plateau for the two-phase reaction where small amount of P2 still exists (Fig. 4b). Choosing 4/9 for P2 is due to a redox related consideration in our computation, as Ni and Mn both reach 4+ at this composition and no more TM redox can be used, which corresponds well with the experimental XAS result for MgNiFeMn (Fig. 6 and Fig. 7). The P2 structure in our DFT simulation shows a 0.8 eV band gap between the HOMO and LUMO, which corresponds to unhybridized 2p orbital and Ni-O hybridized orbital, respectively. This suggests that P2 has a semiconductor-like electronic structure, so the Fermi level is in the middle of the band gap. However, O2 shows a metallic phase with the Fermi level separating occupied and unoccupied oxygen 2p orbitals. These electronic structures are consistent with our XAS measurement that TM redoxes are used up at the end of the P2 solid solution phase in charge to 4.3 V, and further extraction of electrons has to be from oxygen 2p orbitals.

Here we propose a new mechanism to explain the charge-discharge asymmetry in MgNiFeMn. Fig. 9c shows the band structures of O2 and P2 before they contact each other. In the O2 band structure, the energy difference between the highest unhybridized oxygen 2p orbital and Fermi level is 0.2 eV, and the gap between unhybridized 2p orbital and Ni-O hybridized orbital is 0.94 eV. In the P2 structure, the Fermi level is in the middle of the 0.8 eV band gap. As both phases are in the $Na_xMg_{2/9}Ni_{1/9}Mn_{2/3}O_2$ layered crystal, it is suitable to align them using the Fermi level. Thus, when the metallic O2 and semiconductor P2 contact with each other, a 0.4 eV Schottky barrier forms together with the band bending effect and space charge, as illustrated in Fig. 9d.

This energy barrier at the boundary between O2 and P2 phase will only block electron movement from P2 side to O2 side rather than the opposite direction. Since Na ions and electrons move together to preserve local charge neutrality, Na ion movement from P2 toward O2 is also impeded. This unidirectional electronic and ionic barrier gives the asymmetry between charge and discharge. This is because although in discharge, the Na ions from electrolyte can enter into the cathode material through either P2 or O2 phase region, most of the Na ions should choose the P2 side to enter due to the much faster Na conduction than O2 [17]. The Na diffusion barrier for P2 and O2 are calculated to be 140

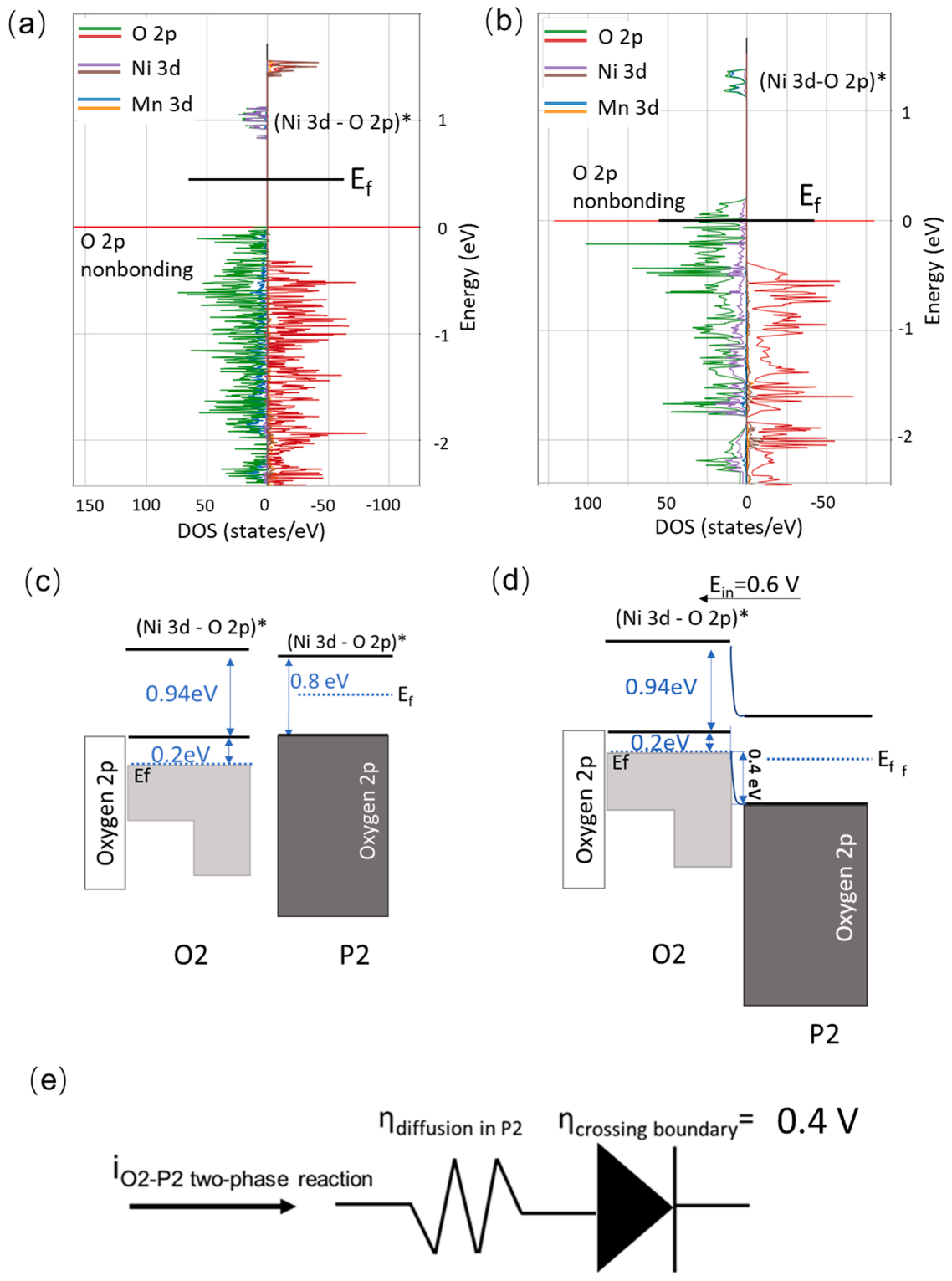

Fig. 9. Electronic structure difference between P2 and O2 phases for the Schottky electron barrier at the phase boundary. (a, b) DOS of (a) P2-$Na_{4/9}Mg_{2/9}Ni_{1/9}Mn_{2/3}O_2$ and (b) O2-$Na_{2/9}Mg_{2/9}Ni_{1/9}Mn_{2/3}O_2$ phases with Na composition of 4/9 and 2/9, respectively. The horizontal red lines at 0 eV label the highest occupied states and horizontal black lines label the Fermi level. **(c)** Schematic illustration of the band structures of O2 and P2 phase before forming the contact, and **(d)** after forming the contact and band bending, giving a 0.4 eV Schottky barrier for electrons moving from P2 to O2. **(e)** Process for typical O2-P2 two-phase reaction represented by a circuit model. The resistance models the Na ion and electron transfer overpotential in P2 and the diode represents the Schottky barrier over the phase boundary from P2 to O2.

meV and 270 meV at the $Mg_{2/9}Ni_{1/9}Mn_{2/3}$ composition in our DFT simulations. Since a typical two-phase reaction occurs by phase boundary sweeping, the Na ions entering the P2 region must further cross the phase boundary, hopping from P2 into O2, in order to transform O2 back to P2 in discharge. However, in the presence of the additional 0.4 eV or 400 meV kinetic barrier across the two-phase boundary, the thermodynamically preferred two-phase reaction is impeded in discharge, giving a sluggish phase boundary movement and a kinetically preferred coexistence of P2 solid solution reaction. This explains why the system in discharge goes through simultaneous P2 solid solution and O2-P2 two-phase reactions. Note that the barrier does not exist if the Na ion and electron move from O2 to P2, which is the allowed hopping direction in charge in addition to the direct dissolution into electrolyte, to grow O2 region with lower Na composition and consume P2 region with higher Na composition, thus giving a conventional P2-O2 two-phase reaction in charge above 4.3 V.

3. A general model for competing kinetics in electrode reactions and design opportunities

For a more precise electrochemistry description, we use the relation of voltage and overpotential to deduce a more general condition for the occurrence of asymmetry between charge and discharge. By definition, the thermodynamically preferred battery reaction releases highest Gibbs free energy among all possible reactions, which means the highest equilibrium voltage E^{eq} from Nernst equation. From electrochemistry, it is known that an activation overpotential for charging or underpotential η (>0) for discharging away from equilibrium voltage is needed for generating certain current. η is contributed by each step of an electrochemical process, such as Na ion and electron transfer through cathode particle. The 0.4 eV electron diffusion barrier at two-phase boundary definitely contributes to the η for the two-phase reaction. Other processes, such as electron transfer through circuit and carbon black and Na ion transfer through electrolyte, all contribute to the iR drop that can be seen in every sub-cycle of a galvanostatic intermittent titration technique (GITT) test. But they are not discussed here as they are not activation energies.

The more kinetically favorable the discharge reaction is, the less underpotential it requires. The discharge working voltage is given by $E = E^{eq} - \eta_{th}$. Assume the kinetically preferred reaction-related quantities are with subscript "k" (e.g., P2 solid-solution reaction in discharge) and the thermodynamically preferred ones are with subscript "th" (e.g., O2-P2 two-phase reaction in discharge). Thus, $E_{th} = E_{th}^{eq} - \eta_{th}$ and $E_k = E_k^{eq} - \eta_k$. Because thermodynamically preferred reaction might not be the most kinetically favored, here it is reasonable to assume that $E_{th}^{eq} \geq E_k^{eq}$ and $\eta_{th} \geq \eta_k$. However, if E_{th}^{eq} is only slightly larger than E_k^{eq} but η_{th} is much larger than η_k, E_{th} can be even larger than E_k.

In our MgNiFeMn material, during discharge, the thermodynamically preferred reaction is O2-P2 two-phase reaction and the other reaction is P2 solid solution. We can estimate E, E^{eq} and η from a GITT test, which is shown in Figure S6. Because the information for two-phase reaction and P2 solid solution reaction is mixed during discharge, we can read the information from charge, where the two reactions are separated. For P2 solid solution, E_k^{eq} ranges from 2.8 V ~ 4.26 V, and η, which is mainly contributed by Na diffusion in cathode particle, is extracted from the voltage relaxation after iR drop to be on the order of ~20 meV at 0.1C. Thus, the range of working voltage E for P2 solid solution in discharge in the same Na composition range is estimated to be E_k = 4.24V-2.78 V.

For a typical P2-O2 two-phase reaction with Na ion and electron smoothly crossing the phase boundary, we can also use the same way to estimate the overpotential, but it is different in the case of O2-P2 two-phase reaction during discharge here since there is an energy barrier for electron to transfer from P2 to O2. Instead, as shown in Fig. 9e, the overpotential here can be represented by a circuit with resistance modeling the Na ion and electron transfer overpotential, and with a diode modeling the unidirectional Schottky barrier at the phase boundary. It is in forward bias condition for electron to move from semiconductive P2 side to metallic O2 side. To construct constant forward bias current, a voltage drop of 0.4 eV will appear to overcome the built-in electric field, which adds up to the overpotential.

For the two-phase reaction of interest here in discharge, E_{th}^{eq} = 4.24 V, η_{th} ~ 0.4 V, thus E_{th} ~ 4.24 V - 0.4 V = 3.84 V, making the E_{th} inside the E_k range from 4.24 V to 2.78 V. Therefore, P2 solid solution reaction will definitely happen simultaneously with two-phase reaction during discharge. The coupling of the two reactions through the Schottky barrier is the main reason for the missing voltage plateau in discharge. In addition, the electric field might be uneven over the phase boundary due to uneven Na distribution and different boundary construction, so some position might have smaller overpotential and some might have larger one, which can spread the working voltage of the two-phase reaction. Also, at the edge of the particle, Na can diffuse through a shorter distance in O2 to the phase boundary and facilitate two-phase reaction. Therefore, although the two-phase reaction in principle happens at a fixed voltage that is indicated by a plateau, here in the discharge of MgNiFeMn it instead can be merged with P2 solid solution to form a high voltage slope region.

In comparison, there are cases where E^{eq} plays a more important role than η, such as Na_xNiO2[24] and Na_xMnO2[7,25] (below 3.6 V) with many Na ordering two-phase reactions but still remain charge-discharge symmetry. For these materials two-phase reaction is thermodynamically preferred, which requires the phase boundary movement of Na orderings by adjusting many Na ions, but solid solution does not involve such a boundary movement, which means solid solution is still kinetically preferred. One related famous example in LIB is the low-rate two-phase reaction transforms to high-rate kinetic driven solid solution reactions in $LiFePO_4$[26,27]. But Na ordering phases usually have steep free energy curves in a phase diagram, which means solid solution reaction from a Na ordering phase will require the change of E_k^{eq} drastically from E_{th}^{eq}, which is not possible most of the time and thus the system reserves the charge-discharge symmetry.

4. Conclusions

In summary, this is the first demonstration that electronic Schottky barrier, rather than conventional purely ionic ones, can form spontaneously and intertwine with the phase boundary evolution in sodium cathode particles. Such a barrier is electronic in nature and emerges and disappears upon battery cycling without requiring irreversible rearrangement of atomic positions. Although the discharge voltage of MgNiFeMn is already much higher than the parent material of MgMn in our work, our general model description here suggests that there are plenty of kinetic design opportunities in tuning dynamic evolution of electronic structures for high-performance Na-ion cathode compounds with further enhanced discharge voltages and reduced polarizations.

Author contributions

X.L. conceived the project and supervised all aspects of the research. Y.W. and Y.L. synthesized the cathode materials. Y.W. performed electrochemical measurements and conducted XRD characterization. Y.W. and X.C. performed DFT calculation. Z. S., E. H. S-J. L. and J-S. L. performed XAS characterization. Y.W. and F. W. performed TEM characterization. X.L., Y.W., and W. F. built the Schottky barrier model. Y.W. and X.L. analyzed the results and wrote the manuscript.

Declaration of Competing Interest

The authors declare that they have no known competing financial interests or personal relationships that could have appeared to influence the work reported in this paper.

Data availability

Data will be made available on request.

Acknowledgements

This work was supported by Meta Platforms, Harvard Climate Change Solutions Fund, and Harvard Data Science Initiative Fund. The TEM experiment was conducted at the MRSEC Shared Experimental Facilities at MIT, supported by the National Science Foundation under award number DMR-14–19807. This work was supported by computational resources from the Extreme Science and Engineering Discovery Environment (XSEDE). The work at Brookhaven National Laboratory was supported by the Assistant Secretary for Energy Efficiency and Renew-able Energy, Vehicle Technology Office of the U.S. Department of Energy through the Advanced Battery Materials Research (BMR) Program under contract DE-SC0012704. This research used resources at beamline 7-BM (QAS) of the National Synchrotron Light Source II, a U.S. Department of Energy (DOE) Office of Science User Facility operated for the DOE Office of Science by Brookhaven National Laboratory under Contract No. DE-SC0012704. The soft X-ray absorption measurements were carried out at the SSRL (beamline 13–3), SLAC National Accelerator Laboratory, supported by the U.S. Department of Energy, Office of Science, Office of Basic Energy Sciences under Contract No. DE-AC02–76SF00515.

Supplementary materials

Supplementary material associated with this article can be found, in the online version, at doi:10.1016/j.ensm.2022.12.027.

Reference

[1] C. Vaalma, D. Buchholz, M. Weil, S. Passerini, A cost and resource analysis of sodium-ion batteries, Nature Rev. Mater. 3 (2018) 18013.
[2] C. Delmas, Sodium and sodium-ion batteries: 50 years of research, Adv. Energy Mater. 8 (2018), 1703137.
[3] N. Yabuuchi, M. Kajiyama, J. Iwatate, H. Nishikawa, S. Hitomi, R. Okuyama, R. Usui, Y. Yamada, S. Komaba, P2-type Nax[Fe1/2Mn1/2]O2 made from earth-abundant elements for rechargeable Na batteries, Nat. Mater. 11 (2012) 512–517, https://doi.org/10.1038/nmat3309.
[4] X. Li, Y. Wang, D. Wu, L. Liu, S.-.H. Bo, G. Ceder, Jahn–Teller assisted na diffusion for high performance Na Ion batteries, Chem. Mater. 28 (2016) 6575–6583, https://doi.org/10.1021/acs.chemmater.6b02440.
[5] X. Li, D. Wu, Y.-.N. Zhou, L. Liu, X.-.Q. Yang, G. Ceder, O3-type Na (Mn0.25Fe0.25Co0.25Ni0.25)O2: a quaternary layered cathode compound for rechargeable Na ion batteries, Electrochem. Commun. 49 (2014) 51–54, https://doi.org/10.1016/j.elecom.2014.10.003.
[6] X. Chen, S. Hwang, R. Chisnell, Y. Wang, F. Wu, S. Kim, J.W. Lynn, D. Su, X. Li, Reversible flat to rippling phase Transition in Fe containing layered battery electrode materials, Adv. Funct. Mater. 28 (2018), 1803896.
[7] X. Chen, Y. Wang, K. Wiaderek, X. Sang, O. Borkiewicz, K. Chapman, J. LeBeau, J. Lynn, X. Li, Super charge separation and high voltage phase in NaxMnO2, Adv. Funct. Mater. 28 (2018), 1805105.
[8] N. Yabuuchi, K. Kubota, M. Dahbi, S. Komaba, Research development on sodium-ion batteries, Chem. Rev. 114 (2014) 11636–11682.
[9] J.L. Kaufman, J. Vinckevičiūtė, S. Krishna Kolli, J. Gabriel Goiri, A. Van der Ven, Understanding intercalation compounds for sodium-ion batteries and beyond, Philos. Trans. R. Soc. A 377 (2019), 20190020.
[10] C. Delmas, C. Fouassier, P. Hagenmuller, Structural classification and properties of the layered oxides, Physica B+ c 99 (1980) 81–85.
[11] N. Yabuuchi, R. Hara, K. Kubota, J. Paulsen, S. Kumakura, S. Komaba, A new electrode material for rechargeable sodium batteries: p2-type Na 2/3 [Mg 0.28 Mn 0.72] O 2 with anomalously high reversible capacity, J. Mater. Chem. A 2 (2014) 16851–16855.
[12] U. Maitra, R.A. House, J.W. Somerville, N. Tapia-Ruiz, J.G. Lozano, N. Guerrini, R. Hao, K. Luo, L. Jin, M.A. Pérez-Osorio, Oxygen redox chemistry without excess alkali-metal ions in Na 2/3 [Mg 0.28 Mn 0.72] O 2, Nat. Chem. 10 (2018) 288.
[13] N. Tapia-Ruiz, W.M. Dose, N. Sharma, H. Chen, J. Heath, J.W. Somerville, U. Maitra, M.S. Islam, P.G. Bruce, High voltage structural evolution and enhanced Na-ion diffusion in P2-Na 2/3 Ni 1/3− x Mg x Mn 2/3 O 2 (0≤ x≤ 0.2) cathodes from diffraction, electrochemical and ab initio studies, Energy Environ. Sci. 11 (2018) 1470–1479.
[14] B. Song, E. Hu, J. Liu, Y. Zhang, X.-.Q. Yang, J. Nanda, A. Huq, K. Page, A novel P3-type Na 2/3 Mg 1/3 Mn 2/3 O 2 as high capacity sodium-ion cathode using reversible oxygen redox, J. Mater. Chem. A 7 (2019) 1491–1498.
[15] E. Boivin, R.A. House, M.A. Pérez-Osorio, J.-.J. Marie, U. Maitra, G.J. Rees, P. G. Bruce, Bulk O2 formation and Mg displacement explain O-redox in Na0. 67Mn0. 72Mg0. 28O2, Joule 5 (2021) 1267–1280.
[16] N. Yabuuchi, R. Hara, M. Kajiyama, K. Kubota, T. Ishigaki, A. Hoshikawa, S. Komaba, New O2/P2-type Li-excess layered manganese oxides as promising multi-functional electrode materials for rechargeable Li/Na batteries, Adv. Energy Mater. 4 (2014), 1301453.
[17] D.H. Lee, J. Xu, Y.S. Meng, An advanced cathode for Na-ion batteries with high rate and excellent structural stability, PCCP 15 (2013) 3304–3312.
[18] X. Wang, G. Liu, T. Iwao, M. Okubo, A. Yamada, Role of Ligand-to-Metal charge transfer in O3-Type NaFeO2–NaNiO2 solid solution for enhanced electrochemical properties, J. Phys. Chem. C 118 (2014) 2970–2976, https://doi.org/10.1021/jp411382r.
[19] S. Xu, Y. Wang, L. Ben, Y. Lyu, N. Song, Z. Yang, Y. Li, L. Mu, H.T. Yang, L. Gu, Fe-based tunnel-type Na0. 61 [Mn0. 27Fe0. 34Ti0. 39] O2 designed by a new strategy as a cathode material for sodium-ion batteries, Adv. Energy Mater. 5 (2015), 1501156.
[20] W.E. Gent, K. Lim, Y. Liang, Q. Li, T. Barnes, S.-.J. Ahn, K.H. Stone, M. McIntire, J. Hong, J.H. Song, Coupling between oxygen redox and cation migration explains unusual electrochemistry in lithium-rich layered oxides, Nat. Commun. 8 (2017) 2091.
[21] G. Assat, J.-.M. Tarascon, Fundamental understanding and practical challenges of anionic redox activity in Li-ion batteries, Nature Energy 3 (2018) 373.
[22] E. Boivin, R.A. House, J.J. Marie, P.G. Bruce, Controlling iron versus oxygen redox in the layered cathode Na0. 67Fe0. 5Mn0. 5O2: mitigating voltage and capacity fade by Mg substitution, Adv. Energy Mater. (2022), 2200702.
[23] E. McCalla, A.M. Abakumov, M. Saubanère, D. Foix, E.J. Berg, G. Rousse, M.-. L. Doublet, D. Gonbeau, P. Novák, G. Van Tendeloo, Visualization of OO peroxo-like dimers in high-capacity layered oxides for Li-ion batteries, Science 350 (2015) 1516–1521.
[24] P. Vassilaras, X. Ma, X. Li, G. Ceder, Electrochemical properties of monoclinic NaNiO2, J. Electrochem. Soc. 160 (2013) A207–A211.
[25] X. Li, X. Ma, D. Su, L. Liu, R. Chisnell, S.P. Ong, H. Chen, A. Toumar, J.C. Idrobo, Y. Lei, J. Bai, F. Wang, J.W. Lynn, Y.S. Lee, G. Ceder, Direct visualization of the Jahn-Teller effect coupled to Na ordering in Na5/8MnO2, Nat. Mater. 13 (2014) 586–592, https://doi.org/10.1038/nmat3964.
[26] B. Kang, G. Ceder, Battery materials for ultrafast charging and discharging, Nature 458 (2009) 190–193.
[27] H. Liu, F.C. Strobridge, O.J. Borkiewicz, K.M. Wiaderek, K.W. Chapman, P. J. Chupas, C.P. Grey, Capturing metastable structures during high-rate cycling of LiFePO4 nanoparticle electrodes, Science 344 (2014), 1252817.